MECHANISMS OF CURRENT PASSAGE AND EFFICIENCY OF SINGLE-JUNCTION AND TANDEM SC BASED ON AMORPHOUS SILICON

A.A. Andreev, V.S. Kalinovsky¶, P.V. Pokrovsky, E. I. Terukov
Ioffe Physical-Technical Institute Russian Academy of Sciences,
26, Polytechnicheskaya, 194021 St. Petersburg, Russia, vitak.sopt@mail.ioffe.ru

ABSTRACT: In the present work, a set of measurements for obtaining dark current-voltage (*J-V*) characteristics of single-junction and tandem SCs based on amorphous and microcrystalline Si was completed. From analysis of obtained forward dark *J-V* characteristics, dominating mechanisms of current flow in the space charge region (SCR) of photovoltaic junctions are determined. On the basis of the experimental data, estimations of the SC efficiency of photovoltaic conversion have been made by the parameters: pre-exponential factor (J_0) and diode coefficient (A) – factor of the junction quality, and comparison with the efficiency obtained from the experimental load *J-V* characteristics. Calculations of the SC efficiency are carried out on the basis of equations correlating the conversion efficiency – (V_η) and the photogenerated current – (J_g) for each portion-segment of the forward dark *J-V* characteristic, which has allowed obtaining the dependence of the efficiency of conversion of optical radiation by a SC on the generation current and estimating a maximum achievable efficiency of the investigated SCs. It has been shown that the method for determining the efficiency of SCs based on the AIIIBV compounds from analysis of forward dark *J-V* characteristics elaborated before is also applicable to such a non-standard semiconductor material as amorphous silicon.

Keywords: Amorphous Silicon, Tandem, *a*-Si/μ-S, Photoelectric properties, Efficiency.

1 INTRODUCTION

At present, solar cells (SCs) based on amorphous silicon are extensively studied. At the same time, no detailed studies and analysis of dark current-voltage (*J-V*) characteristics of amorphous silicon SCs have been performed, with exception of separate publication [1, 2]. Studies of this kind are not systematic and do not relate specific features of dark *J-V* characteristics of structures based on amorphous semiconductor to their efficiency. In this study, we made an attempt to determine the dominant charge transport mechanisms by analysis of dark forward *J-V* characteristics of single-junction *a*-Si:H and tandem μc-Si:H + *a*-Si:H SCs on amorphous silicon, evaluate the potential photoconversion efficiency of such cells on the basis of the thus obtained pre-exponential factor J_{0i} and diode coefficient A (quality factor of the *p-n* junction), and compare this efficiency with experimental results. For this purpose, we used the calculation procedure based on equations that relate the efficiency η and photogeneration current J_g to the parameters A and J_{0i} of dark *J-V* characteristics, first suggested for photovoltaic converters based on III-V materials in [3, 4]. The results of these calculations are compared with the efficiencies found in measurements of light *J-V* characteristics of single-junction (*a*-Si:H) and tandem (*a*-Si:H + μc-Si:H) SCs.

2 SAMPLE FABRICATION TECHNIQUE

The single-junction *p-i-n* structures were fabricated on amorphous silicon by successive deposition of three layers, that doped with boron to the *p*-type, intrinsic *i*-layer, and phosphorus-doped *n*-type layer, onto glass and quartz substrates with a preliminarily deposited current-conducting indium-tin-oxide (ITO) contact layer. Further, a contact layer of aluminum was deposited. The silicon layers were formed in glow-discharge plasma of silane (SiH_4) diluted with hydrogen to 6%. Diborane (B_2H_6) and phosphine (PH_3) gases were introduced into silane for doping to obtain *p*- and *n*-types, respectively. The substrate temperature was 200°C. The whole process was in situ monitored by optical interferometry, which made it possible to determine the thickness of the layers and, to a certain extent, to determine their quality by estimating the relative value of the refractive index of a film being deposited. The thickness of the *p*-layer did not exceed 10 nm, and that of the intrinsic layer, 450 nm.

The process of fabrication of tandem *p-i-n* structures includes successive deposition of two photoactive cascades based on hydrogenated amorphous and micro-crystal silicon. As a substrate for deposition of microamorphic photovoltaic converters served a float-glass with low content of iron. The contact and photoactive layers of the thin-film tandem were deposited in several stages. In the first stage, the layer of the transparent frontal conducting ZnO contact with a thickness of approximately 1.8 μm is formed by the low-pressure chemical vapor deposition (LPCVD) method from a mixture of diethylzinc $Zn(C_2H_5)_2$, water vapor, and diborane B_2H_6 serving as a dopant source. This is done at a temperature of 180°C and a pressure of 0.5 mbar. Then, the cascade based on amorphous silicon is deposited: *p*-doped *a*-SiC:H, intrinsic *a*-Si:H, and *n*-doped *a*-Si:H. With addition of carbon, it is possible to make the energy gap of the *p*-type layer wider and to diminish the parasitic absorption of light in this layer. The thickness of the amorphous cascade is 200-250 nm, and that of each of the doped layers, 15-20 nm. The deposition is by the plasma-enhanced chemical vapor deposition (PECVD). As the main reactants serve silane SiH_4 and hydrogen. Methane CH_4 is used as a source of carbon, and trimethylboron $B(CH_3)_3$, as that of the doping impurity. The deposition is performed at a temperature of 200°C, pressure of 0.5 mbar, high-frequency discharge power of 200-400 W, and discharge frequency of 40.7 MHz. After the amorphous cascade is formed, the single-crystal silicon cascade is deposited. The monolithic connection between the cascades is provided by a tunnel junction constituted by successively deposited *n*-doped layer of the amorphous cascade and the *p*-doped layer of the micro-crystal cascade. The thickness of the micro-crystal cascade is within 1-1.5 μm. The cascade is constituted by *p*-, *i*-, and *n*-type layers. The larger thickness of the micro -crystal cascade is due

to the smaller optical absorption coefficient of micro-crystal silicon, compared with amorphous silicon. As reactants serve the same gases as those in deposition of the amorphous cascade, but their relative flow rates, plasma discharge power, and working pressure are changed. The deposition is performed at a temperature of 160°C, pressure of 2.5 mbar, high-frequency discharge power of (0.16-0.26) W/cm^2, and discharge frequency of 40.7 MHz. Then, the rear transparent conducting ZnO contact is deposited by the method similar to that for the frontal contact. The rear contact is somewhat thinner than the frontal contact because of the higher doping level.

We studied dark and light *J-V* characteristics of single-junction (*a*-Si:H) and tandem (*μc*-Si:H + *a*-Si:H) solar cells with areas of 0.05 to 2 cm^2. It is noteworthy that we did not pursue the goal of fabricating cells with the maximum efficiency. The efficiencies of the single-junction *a*-Si:H cells was in the range (4-6)%, and that of *μc*-Si:H + *a*-Si:H tandem cells was about 9%.

3 EXPERIMENTAL RESULTS

The dark *J-V* characteristics were measured by the direct contact method on an installation with automatic recording and processing of results. The external bias was varied from 0 to 3 V. For the main part of the *p-i-n* structures *a*-Si:H structures under study, the forward bias was chosen to be within the range (0-1.5) V.

Light *J-V* characteristics were measured on a solar light simulator. The load *J-V* characteristics measured with the simulator, were correlated with open-sunlight measurements, (~1000 W/m^2).

The experimental dark forward *J-V* characteristics of the *a*-Si:H and *μc*-Si:H + *a*-Si:H samples under study are shown in Fig. 1: curves 1-5, single-junction SCs; (5, 6) tandem cells. For rough estimation purposes, Fig. 1 shows by dashed curves calculated exponentials with diode coefficients $A = 2$ and $A = 1$. It can be seen that the dark *J-V* characteristics of all the samples are constituted by at least three clearly pronounced segments. Within each separate segment of *J-V* characteristics, the experimental dependences are exponential *J-V* characteristics of the form $J_0\exp(eV/AkT)$, with widely varying diode coefficients (diode quality parameters) *A*. The dark *J-V* characteristics of single-junction *a*-Si:H CSs show at bias voltages of 0.55 to 0.75 V a certain "median" segment with a characteristic value of the diode coefficient A = (2-1), which is indicative of a "recombination" (Saah-Noyce-Shockley) and "diffusion" (Shockley) [5, 6] charge transport mechanism in the space charge region (SCR) of the *p-n* junctions studied. Figure 2 presents a detailed fitting to experimental *J-V* characteristics for samples of single-junction *a*-Si:H and tandem *μc*-Si:H + *a*-Si:H SCs. It can be seen that for the *a*-Si:H SC represented by curve 3, the "recombination" charge-transport mechanism $A = 2$ is dominant in the "median" segment, whereas for the sample represented curve 1, a gradual transition from the "recombination" charge-transport mechanism to that of the purely "diffusion" type with $A = 1$ is observed with increasing forward bias. The experimental dark forward *J-V* characteristic of the *μc*-Si:H + *a*-Si:H tandem (curve 7 in Fig. 1 and curve 5 in Fig. 2) has the following specific features: the "median" segment is extended along the voltage scale to higher voltages and the diode coefficient in the beginning part of the segment is twice the coefficient for the "recombination" portion of the single-junction *a*-Si:H SC, i.e., $A = 4$ (Fig.2), and it approaches ~ 2.5 with increasing voltage. In terms of the model suggested in [3, 4], this corresponds to the following: the diode coefficient of the multiple-junction SC is arithmetic sum of the coefficients of all the constituent photoactive junctions ($A = A_1 + A_2 + \dots A_n$) and the pre-exponential factor J_0 is geometric mean $J_0 = \sqrt[n]{J_{0_1} \cdot J_{0_2} \cdot \dots \cdot J_{0_n}}$ of their pre-exponential coefficients. Thus, we have, at the beginning of the "median" segment of the *J-V* characteristic for, e.g., the *μc*-Si:H + *a*-Si:H tandem cell (Fig. 2), the "recombination" mechanism of charge transport in the space charge regions of its photoactive *p-i-n* diodes ($A = 4$ and $J_{0r} = 1.3\ 10^{-9}$ A/cm^2). In the end of the "median" segment, we have a "quasi-diffusion" mechanism is operative, i.e., the "diffusion" mechanism with a remainder of that of the "recombination" type ($A = 2.5$ and $J_0 = 1\ 10^{-11}$ A/cm^2. Based on the values of the pre-exponential factor J_{0r} = (1 10^{-9}-2 10^{-11}) A/cm^2, obtained by fitting to the experimental dark *J-V* characteristics for single-junction *a*-Si:H SCs (Tables 1 and 2), we can estimate the pre-exponential factor J_{0r} for the "recombination" mechanism for the *μc*-Si:H photoactive junction in the *μc*-Si:H + *a*-Si:H tandem cell under study, i.e., $J_{0r} \approx$ (8 10^{-8}-1.7 10^{-9}) A/cm^2.

It follows from a comparison of the *J-V* characteristics for the whole set of samples that all the curves are qualitatively similar and only differ in particular parameters of their segments: *A* and J_0. The general form of the curves on the whole corresponds to the "classical" *J-V* characteristics for the *p-n* junction [7]. The *J-V* characteristic contains three clearly pronounced segments. The initial, "tunnel-trap," segment is observed at low voltages up to (0.3-0.4) V and characterized by an

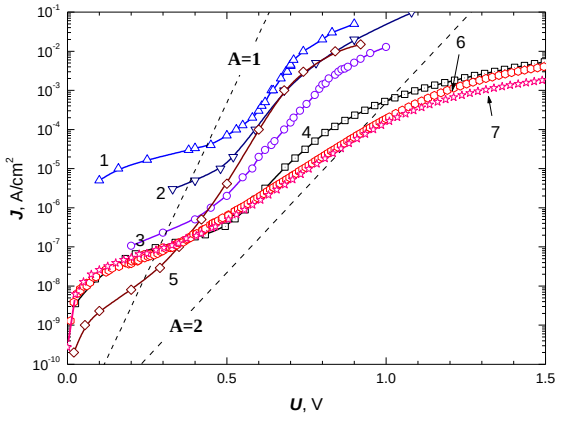

Figure 1: Experimental forward dark *I-V* characteristics of single-junction *a*-Si:H SCs (curves 1–5) and of tandems *μ*c-Si:H + *a*-Si:H (curves 6 and 7) obtained from measurements at room temperature.

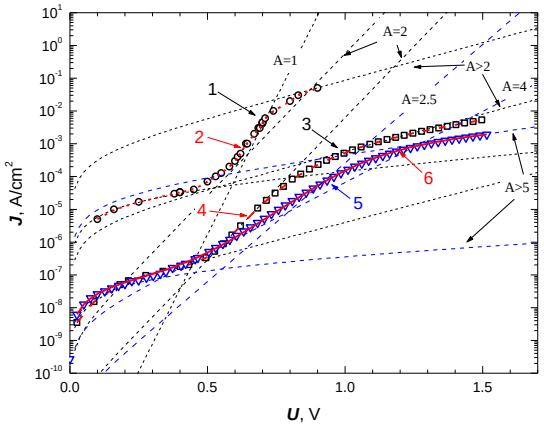

Figure 2: Experimental and rated forward dark *J-V* characteristics of two single-junction *a*-Si:H SCs (curves 1 and 3) and of a tandem *μ*c-Si:H + *a*-Si:H (curve 5); curves 1, 3 and 5 – experiment (at room temperature); curves 2, 4 and 6 – calculation. Curve 1 in Fig.2 contains 4 exponential portions: "tunnel-trap" one with $A > 2$, $J_{0(A>2)} = 3.0 \cdot 10^{-5}$ A/cm^2; "recombination" – $A = 2$, $J_{0(A=2)} = 1.2 \cdot 10^{-9}$ A/cm^2; "diffusion" – $A = 1$, $J_{0(A=1)} = 7.6 \cdot 10^{-15}$ A/cm^2; and "superinjections" – $A > 2$, $J_{0(A>2)} = 4.5 \cdot 10^{-4}$ A/cm^2. Curve 3 contains 3 exponential portions: "tunnel-trap" – $A > 2$, $J_{0(A>2)} = 2.7 \cdot 10^{-8}$ A/cm^2; "recombination" – $A = 2$, $J_{0(A=2)} = 1.3 \cdot 10^{-11}$ A/cm^2 and "superinjections" – $A > 2$, $J_{0(A>2)} = 3.0 \cdot 10^{-6}$ A/cm^2. Curve 5 contains 4 exponential portions: "tunnel-trap" – $A > 5$, $J_{0(A>5)} = 2 \cdot 10^{-7}$ A/cm^2; "recombination" – $A = 4$, $J_{0(A=2)} = 1.3 \cdot 10^{-9}$ A/cm^2; "quasi-diffusion" – $A = 2.5$, $J_{0(A>2)} = 1 \cdot 10^{-11}$ A/cm^2 and "superinjections" – $A > 5$, $J_{0(A>5)} = 6.0 \cdot 10^{-7}$ A/cm^2.

exponential {exp(*eV/AkT*)}, diode coefficient $A > 2$, and pre-exponential factor J_0 in the range (3 10^{-5}-6 10^{-9}) A/cm^2. The main, "median," segment observed at voltages of (0.45-0.85 V) for single-junction SCs has A in the range (2-1) and J_{0r} and J_{0d} of (1.2 10^{-9}-2 10^{-11}) and (8 10^{-15}-2 10^{-15}) A/cm^2, respectively. For the tandem samples at voltages of (0.4-1.14 V), the diode coefficient A is (4-2.5) and J_{0r} = (1 10^{-9}-1 10^{-11}) A/cm^2. The third segment, observed at bias voltages higher than (0.8-1.1) V, has $A > 2$ and $J_{0i} = (2.5 \cdot 10^{-3} - 1 \cdot 10^{-7})$ A/cm^2. In the most general case, the "median" segment is interpreted, in accordance with the value of the diode coefficient, A = (2-1), as a result of a "recombination" process supplemented with a "diffusion" contribution. For some of the samples (nos. 5320, 187, 247), this segment can be reliably divided in two, with a clearly pronounced "recombination" component at lower biases and transition, with increasing bias, to pure "diffusion" (Shockley) with a dc $A = 1$. The third segment ($U_c > 0.8$ V and $A > 2$) is commonly defined in some studies [8] as the "superinjection" region and we adopt this terminology. The increase in the parameter $A > 2$ may be due to various mechanisms. These are the following: current limitation by the space charge of injected electrons and holes, uncompensated at the *p-n* junction [8]; emission-tunneling processes in contact regions [9]; and, at even higher voltages creating a field strength E ≈ 10^6 V/cm, "tunneling-field-induced hopping" phenomena of the type of multistage tunneling (Fowler-Nordheim) [8]. Because a solar cell based on amorphous materials operates at voltages of about 1 V, the detailed physical essence of these processes is of no importance for calculating the photovoltaic conversion efficiency. More probably, the third segment is important as an indication that the current rise rate starts to fall. This process is equivalent to an increase in the resistance in the current circuit, although the real physical process is much more complex. As follows from our experimental results, the voltage dependence of the current is described in this segment by an exponential with a quality factor $A >> 2$. Numerous previous studies of the charge transport mechanism in amorphous silicon structures with a *p-n* junction have shown that large values $A >> 2$ are always related to the density of electron states, being specifically due to its large value (DoS > 10^{17} cm^{-3}). If, however, the DoS is lower than this critical value and the *p-n* junction shows a diffusion charge-transport mechanism, then, as the band structure of the junction reaches the flat-band state with increasing bias, the problem of the high density of states again becomes important. In view of the aforesaid, the complex physical processes in the initial part of the third segment, at (1-1.5) V, can be simply simulated by an equivalent ohmic resistance (R_S), whose value is determined by fitting of the calculated *J-V* characteristics to those measured experimentally (Fig. 2). It is important for us to emphasize, in this general description of dark *J-V* characteristics that the "recombination-diffusion process is observed in all the samples under study. This is indicative of the sufficiently good quality of the material of the cells. For amorphous silicon fabricated by an unoptimized method, and also for alloys of amorphous

Table I:

Structure	current flow mechanism							
	tunnel- trap, J_{0t},		U_1	recombi-nation, J_{0r}		U_2	emission-tunnel, J_{0i}	
	A/cm^2	A	V	A/cm^2	A	V	A/cm^2	A
α -Si:H, № 191	3E-8	>2	0.45	1E-11	2	0.83	3E-6	>2
α -Si:H, № 246	8E-7	>2	0.5	5.3E-11	2	0.85	2E-5	>2
α -Si:H, №2916	4E-7	>2	0.45	1E-10	2	0.85	8.6E-6	>2

Table II:

Structure	current flow mechanism									
	tunnel-trap, J_{0t}		U_1	recombination, J_{0r}		diffusion, J_{0d}		U_2	emission-tunnel, J_{0i}	
	A/cm^2	A	V	A/cm^2	A	A/cm^2	A	V	A/cm^2	A
α-Si:H, №5320	6E-9	>2	0.3	9.6E-11	2	3.6E-15	1	0.8	2.5 E-3	>2
α -Si:H, №187	7E-6	>2	0.4	4E-10	2	2.3E-15	1	0.85	5.6E-6	>2
α -Si:H, №247	3E-5	>2	0.45	1.2E-9	2	7.6E-15	1	0.8	4.5E-4	>2
α -Si:H+ *μc*-Si:H, №1C1	2E-7	>5	0.4	1.3E-9	4	1E-11	2.5	1.12	6E-7	>5

Table III:

Structure	current flow mechanism							
	tunnel- trap, J_{0t},		U_1	recomb.-diffuss., J_{0rd}		U_2	emission-tunnel, J_{0i}	
	A/cm^2	A	V	A/cm^2	A	A/cm^2	A	V
α -Si:H +μc-Si:H, №1F4	1.5E-7	>5	0.4	1E-9	3	1.14	8.8E-7	>5
α -Si:H +μc-Si:H, №1C2	1.6E-7	>5	0.4	1E-9	3	1.14	1.8E-7	>5
α -Si:H +μc-Si:H, № 1A4	1E-7	>5	0.4	8E-10	3	1.14	1E-7	>5

silicon with carbon and some other materials, the quality of the *p-n* junction, as a rule, falls and the "recombination-diffusion" components of *J-V* characteristics may be unobserved at al. The transport in materials of this kind was considered in [10].

The results of a detailed processing of the experimental forward dark *J-V* characteristics as a sum of segments corresponding to different carrier transport mechanisms in the SCR at various bias voltages are listed in Tables 1, 2, and 3. Table 1 characterizes the parameters of the single-junction structures with dominant "recombination" mechanism of charge transport in the SCR of the *p-i-n* junction in the "median" segment of the dark *J*-V characteristics. Table 2 lists the parameters of the single-junction structures and tandem with a "recombination" mechanism predominant at the beginning of the "median" segment, and the "diffusion" mechanism at its end. Table 3 summarizes the parameters of the tandem cells in which both the "recombination" and "diffusion" mechanisms of charge transport in the SCR of the photovoltaic *p-i-n* junctions are operative in the "median" portion of the ark *J-V* characteristic.

Figure 3 shows light *J-V* characteristics of the single-junction and tandem SC samples under study. The optimal-load efficiencies (represented by squares in Figs 4, 5, and 6) calculated from the light *J-V* characteristics are used in what follows in comparison with the calculated efficiencies. It can be seen in Figs. 4 and 5 that the experimental efficiencies for single-junction *a*-Si:H samples (squares 5) lie lower than the calculated potential values (curves 3 and 4).

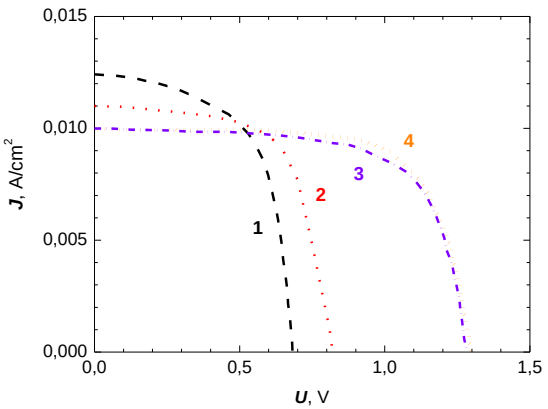

Figure 3: Experimental light *J-V* characteristics of single-junction *a*-Si:H SCs (curves 1, 2) and of tandems μc-Si:H+*a*-Si:H (curves 3,4) obtained from measurements at room temperature, irradiation AM1.5.

As already noted, this result is expected because the calculation disregards the reflection loss and some other aspects of the post-growth processing of single-junction SCs.

4 ESTIMATION OF PHOTOCONVERSION PARAMETERS FROM DARK *J-V* CHARACTERISTICS

As shown in studies concerned with III-V SCs, dark *J-V* characteristics may be rather informative in estimation and prognostication of parameters of photovoltaic converters of this kind [3, 4]. The authors introduce into consideration for subsequent analysis a common functional dependence for the dark forward *J-V* characteristic, which includes all the experimentally observed segments of *J-V* characteristics, identified as the corresponding segments of the entire curve. The *J-V* characteristic was obtained by summation of the components corresponding to different segments of the *J-V* characteristics.

$$J = J_{0t}(\exp V_\varphi / A_t\varepsilon - 1) + J_{0r}(\exp V_\varphi / A_r\varepsilon - 1) + J_{0d}(\exp V_\varphi / A_d\varepsilon - 1) \quad (1)$$

The dark zero-resistance *J*-V_φ characteristic (1) can be approximated with three segments, for each of which the dependence of the voltage in the SCR on the dark current has the form [3]:

$$V_\varphi = A\varepsilon \cdot \ln(J / J_0 + 1) \quad (2)$$

This "segmental approximation" enables smoothing of the calculated functional *J-V* characteristic by mathematical averaging of values of *J-V* characteristics in regions of matching between various segments. As demonstrated by the experience gained in working with such a calculated curve, it proves highly useful in analytical data processing and becomes simply necessary for multiple-junction structures (tandem etc.) In the general case, in the matching region of the segments of *J-V* characteristics, the "voltage-" and "current-related" boundaries between the neighboring segments are given by

$$\begin{cases} V_{n(n+1)} = \dfrac{A_n A_{(n+1)}}{A_n - A_{(n+1)}} \varepsilon \cdot \ln(J_{0n} / J_{0(n+1)}) \\ J_{n(n+1)} = \dfrac{J_{0n}^{A_n/(A_n - A_{(n+1)})}}{J_{0(n+1)}^{A_{n+1}/(A_n - A_{(n+1)})}} \end{cases} \quad (3)$$

where n and $(n + 1)$ are the indices of neighboring segments.

The light *J-V* characteristic (for simplicity, we restrict our consideration to single segment) is obtained from the corresponding segment of the dark *J-V* characteristic and has the form $J = J_g - j$

$$\begin{cases} V_\varphi = A\varepsilon \ln\left(\dfrac{(J_g - j)}{J_0}\right) \\ j = J_g - J_0 \exp\left(\dfrac{V_\varphi}{A\varepsilon}\right) \end{cases} \quad (4)$$

where $\varepsilon = kT/q$.

In the open-circuit mode, $j = 0$ and $V = V_{OC}$. Then (4) gives the equation

$$J_g = J_0 \exp\left(\frac{V_{oc}}{A\varepsilon}\right) \quad (5)$$

which has the same pre-exponential factor as the corresponding segment of the dark *J-V* characteristic and coincides in form with the expression for the dark *J-V* characteristics. The same is true for the continuous function of conjugated segments.

Further, to estimate the photoconversion parameters, it is necessary to correlate the efficiency of a solar cell with the generation current. The full set of equations describing this correlation was given in [3,4]. We only describe here the physical aspect of this analysis. The derivative of the power ($J \cdot V_\varphi$) from Eqs. (4) at the optimal-load point is zero. Solution of the transcendental equation yields the expressions.

$$\begin{cases} V_{oc} = V_m + E \ln\left(1 + \dfrac{V_m}{E}\right) \\ \left(1 + \dfrac{V_m}{E}\right)\exp\left(\dfrac{V_m}{E}\right) = \exp\left(\dfrac{V_{oc}}{E}\right) \end{cases} \quad (6)$$

where $E \equiv A\varepsilon$ and, using the rearrangements made in [3, 4], we find the maximum power generated by the cell at the optimal-load point

$$P_m = J_g \cdot V_m^2 / (V_m + E) \quad (7)$$

Then the efficiency

$$\eta = J_m V_m / P_{inc} = \frac{J_g}{P_{inc}} \cdot \frac{V_m^2}{V_m + E} = \frac{V_\eta}{V_{conv}} \quad (8)$$

Because the ratio between the incident power (P_{inc}) and the generation current at a fixed solar radiation spectrum, $\frac{P_{inc}}{J_g} = V_{conv}$, is independent of the radiation intensity, the full dependence of the efficiency η on the generation current J_g proportional to the solar light concentration can be expressed in terms of the parameter – (V_η) defined as "efficiency" voltage [3, 4] equal to

$$V_\eta \equiv \frac{V_m^2}{V_m + E} \quad (9)$$

Using relation (9), we can express J_g in terms of V_η and obtain a full expression for the dependence $J_g - \eta(\propto V_\eta)$ for the whole set of segments of the *J-V* characteristic of the photovoltaic converter. The effect of the series resistance R_S of the whole structure (contact resistance and that of the tunnel junction) is taken into account by introduction of the correcting equation $V_{\eta o} = V_\eta + R_S$. The calculations are made by using the special program on the basis of the expressions presented in the communication and the data obtained by fitting to the experimental dark *J-V* characteristics of the single-junction and tandem SCs studied.

The results of these calculations for single-junction *a*-Si:H and *μc*-Si:H + *a*-Si:H tandem samples (Fig. 2) are presented in Figs. 4, 5, and 6, which combine the dark forward *J-V* and generation current-efficiency (J_g-η) characteristics of the samples studied.

It can be seen that, for the samples studied, the $J_g - \eta$ characteristics (curves 3, 4) are constituted by the same segments as the dark forward *J-V* characteristics (curves 1, 2) (Figs. 4, 5, 6). For the *a*-Si:H SC sample in Fig. 4, the potential efficiency (curve 3) is limited in the working range of current densities by the "recombination" charge transport mechanism (A = 2), and for the *a*-Si:H SC sample in Fig. 5, by the "diffusion" mechanism (A =1), which accounts for the somewhat higher experimental and calculated values of the efficiency for the second sample. For the *μc*-Si:H+*a*-Si:H tandem SC sample, the potential efficiency (Fig. 6, curve 3) is limited by the "quasi-diffusion" mechanism (A = 2.5), i.e., by the "diffusion" mechanism with remainder of the "recombination" charge-transport mechanism. The calculated curve 4 obtained using the parameters A, J_0, and R_S found by fitting to the dark *J-V* characteristic well coincides with the experimental efficiency found from the light *J-V* characteristic (Fig. 3, curve 5) [designated by square (5) in the plot].

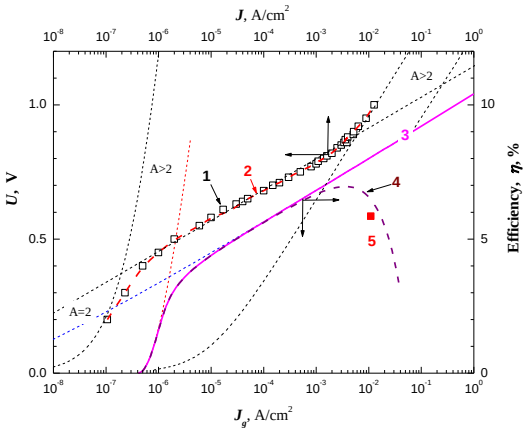

Figure 4: Experimental and calculated characteristics of single-junction *a*-Si:H SC: forward dark *J-V* characteristic: 1-experiment, 2-calculated; generation current (J_g) — SC efficiency (η): 3, 4-calculated (R_s = 0, R_s ~ 5 Ohm*cm^2), 5 - experiment, (AM1.5). Segments of the characteristics: A > 2, $J_{0(A>10)}$ = 4.1·10^{-7}A/cm^2; A = 2, $J_{0(A=2)}$ = 1.15·10^{-10} A/cm^2; A > 2, $J_{0(A>2)}$ = 8.6·10^{-6} A/cm^2.

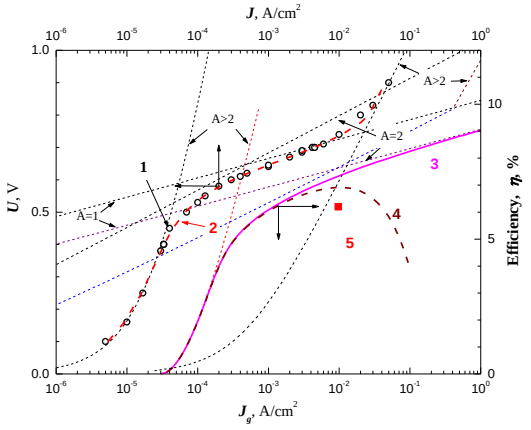

Figure 5: Experimental and calculated characteristics of single-junction *a*-Si:H SC: forward dark *J-V* characteristic: 1-experiment, 2-calculated; generation current (J_g) — SC efficiency (η): 3, 4-calculated (R_s = 0, R_s ~ 3.5 Ohm*cm^2), 5 - experiment, (AM1.5). Segments of the characteristics: A > 2, $J_{0(A>2)}$ = 3·10^{-5} A/cm^2; A = 2, $J_{0(A=2)}$ = 1.2·10^{-9} A/cm^2; A = 1, $J_{0(A=1)}$ = 7.6·10^{-15} A/cm^2; A > 2, $J_{0(A>2)}$ = 4.5·10^{-4} A/cm^2.

With increasing current density J_g or illuminance, the influence exerted by the series resistance R_S (Figs. 4, 5, and 6; curves 4) and by the "super-injection" region on

the efficiency η of the SCs we studied becomes important.

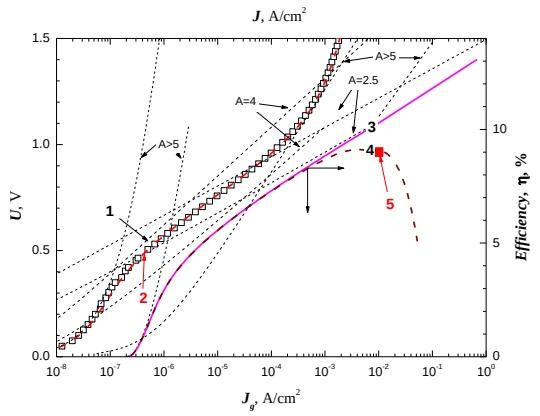

Figure 6: Experimental and calculated characteristics of tandem μc-Si:H + a-Si:H: forward dark J-V characteristic: 1-experiment, 2-calculated; generation current (J_g) — SC efficiency (η): 3, 4-calculated (R_s = 0, R_s ~ 5 Ohm*cm^2), 5 -experiment, (AM1.5). Segments of the characteristics: $A > 4$, $J_{0(A>4)} = 2 \cdot 10^{-7}$ A/cm^2; $A = 4$, $J_{0(A=4)} = 1.3 \cdot 10^{-9}$ A/cm^2; $A = 2.5$, $J_{0(A=2.5)} = 1.3 \cdot 10^{-11}$ A/cm^2; $A > 4$, $J_{0(A>4)} = 6 \cdot 10^{-7}$ A/cm^2.

However, revealing the correlation between the nature of the exponential in the "superinjection" region and SC parameters requires a special study.

Thus, our calculation procedure based on the parameters A, J_0, and R_S, found by analysis of experimental dark forward J-V characteristic, both demonstrates the ultimate potential of the growth technology used in the study and indicates that the opportunities for raising the efficiency of SCs based on amorphous materials are not exhausted.

5 CONCLUSIONS

It was shown that dark forward current-voltage (J-V) characteristics for p-i-n structures based on amorphous hydrogenated silicon are of key importance for evaluation the photoconversion efficiency of a-Si:H solar cells (SCs). Measurements and analysis of dark J-V characteristics enables control over, and improvement of the technological process of fabrication of a-Si:H p-i-n structures. This is particularly important for cascaded SCs for which the quality of photoactive p-i-n junctions, balance of currents and resistances of separate components, and other their parameters dependent on post-growth techniques form a complex physical pattern, which is difficult to explain and optimize without understanding of the dominant charge-transport mechanism in the space-charge region of amorphous p-i-n structures, determined by analysis of dark J-V characteristics. Dark J-V characteristics of a broad set of a-Si:H single-junction SCs fabricated with certain differences in the growth technique were measured. Nevertheless, the SCs show similarity between curves of dark J-V characteristics and their characteristic segments and make it possible to reveal the fundamental aspects of charge-transport mechanisms in the SCR of photoactive junctions.

It is of fundamental importance that, in all cases, there are common segments of the dark forward J-V characteristic: of "tunnel-trap" and "emission-tunneling" types with a diode quality factor $A > 2$ for single-junction SCs and $A > 5$ for tandem cells; of "recombination" type with $A = 2$ for single-junction SCs and $A = 4$ for tandems; of "diffusion" type with $A = 1$ for single-junction SCs and "quasi-diffusion" type with $A = 2.5$ for tandem cells. Single-junction cells with these mechanisms of charge transport across the p-n junction have an efficiency of about 6%. This result is characteristic of cell with the simplest structure having no built-in antireflection and light-scattering layers. The tandem cells based on μc-Si:H + a-Si:H p-i-n structures have an efficiency of about 9% and demonstrate ways to improve the efficiency of photovoltaic converters based on amorphous materials.

In the SCs based on a-Si:H and μc-Si:H, the conversion of unconcentrated sunlight is strongly affected by the "recombination" mechanism of charge transport in the SCR of p-i-n junctions.

The method for analysis of experimental dark J-V characteristics, previously suggested and tested for multiple-junction SCs based on III-V crystalline compounds, is also applicable to single- and multiple-junction p-i-n structures based on amorphous hydrogenated silicon and, therefore, it becomes an all-purpose procedure.

6 ACKNOWLEDGMENTS

The authors are grateful to V.M. Andreev, A.C. Gudovskih for support, helpful discussions, and assistance.
The study was supported by the Ministry of education of science of the Russian Federation (state contract no. № 16.516.11.6053) and by a Federal target program (State contract nos. № 16.513.11.3084 и № 16.526.12.6017).

7 REFERENCES

[1] A. Mitiga, P. Fiorini, M. Falconieri, F. Evangelisti, J. Appl. Physics, 66**,** (6), 1989, 2667.
[2] McMahon T.J., Yacobi B.G., Madan A., J. Non Cryst. Solids, 66, 1984, 375.
[3] V.S. Kalinovsky, V.M. Andreev, et al., Proceedings of the 25th European PV Solar Energy Conference and **5**th World Conference on Photovoltaic Energy Coversion, Valencia, Spain, 2010, 979
[4] V.M. Andreev, V.V. Evstropov, V.S. Kalinovsky, V.M. Lantratov, V.P. Khvostikov, Semiconductors, v.43, 5, 2009, 644
[5] W. Shokley, H. J. Queisser, J. Appl. Phys. 32**,** 1961, 510
[6] S.M. Sze, Physics of Semiconductors Devices, John Wiley & Sons, 1981
[7] A. Fahrenbruch, R. Bube, Fundamentals of Solar Cells. Photovoltaic Solar energy conversion, New York, 1983
[8] M.A. Lampert, P. Mark. Current injection in Solids, Academic Press, New York and London, 1970
[9] B.L. Sharma, R.K. Puronit, Semiconductor Heterojunctions, Pergamon press, 1974
[10] A.A. Andreev. Fizika i tekhnika poluprovodnikov, 42, 11, 2008, 1363